European Aluminium Congress 2011

Numerical prediction of thermal panel distortion incorporating thermal material properties of 6016 aluminum alloy

Christoph Albiez [1,a], Mathias Liewald [1,b], Andreas Görres [2,c], Jochen Regensburger [2,d]

[1]Institute for Metal Forming Technology, Holzgartenstraße 17, 70174 Stuttgart, Germany
[2]Audi AG, NSU Straße, 74148 Neckarsulm, Germany

[a]christoph.albiez@ifu.uni-stuttgart.de, mathias.liewald@ifu.uni-stuttgart.de,
[c]andreas.goerres@audi.de, [d]jochen.regensburger@audi.de

Topics: Application-oriented process technologies

Abstract

Challenging automotive design in the face of modern lightweight strategies for weight reduction as well as legislative regulations, impose higher requirements for future car body development. This trend has led to the use of thinner sheet metal blanks and implies the need for narrow process windows especially within the coating process where thermal loads might cause local shape deviations. Moreover, developments in multi-material-design induce material configurations with complex deformation behavior due to different expansion characteristics. For this reason, there is a need to improve the numerical prediction of surface quality in the early car development process. This paper deals with the effect of thermo-mechanical material properties relating to the final part characteristics, whereby the influence of time and heat dependent material properties affecting the yield point and flow characteristics is shown. In further investigations the influence of initial yield strength, pre-stretching and subsequent thermal loads to the final yield strength is dealt with.

Introduction

The development of car body structure is one of the major activities in the automotive manufacturing process. Therefore technical, legislative as well as customer-specific demands lead to far-reaching lightweight efforts. However, there is a conflict between the diversity of variants, higher requirements to the vehicle safety and processing quality on one side and higher demands on comfort, aesthetic and shortening periods of development on the other side.

Fig. 1: Assessment of the surface quality after coating process [Audi]

The essential reduction of costs, weight, fuel consumption and CO2 emission, is only possible through consequent combination of material, shape, manufacturing and construction lightweight concepts. The use of lightweight materials in car body manufacturing process poses new challenges for existing narrow process windows. Due to thermal processes, elastic and plastic deformations of car body parts may lead to time and cost consuming optimization loops in the pre-series phase of a new product.
In addition to the surface quality, thermal processes have an influence on the dimensional accuracy, car body design and functional behavior (NVH) as well as safety aspects concerning the crash performance (Fig. 2).

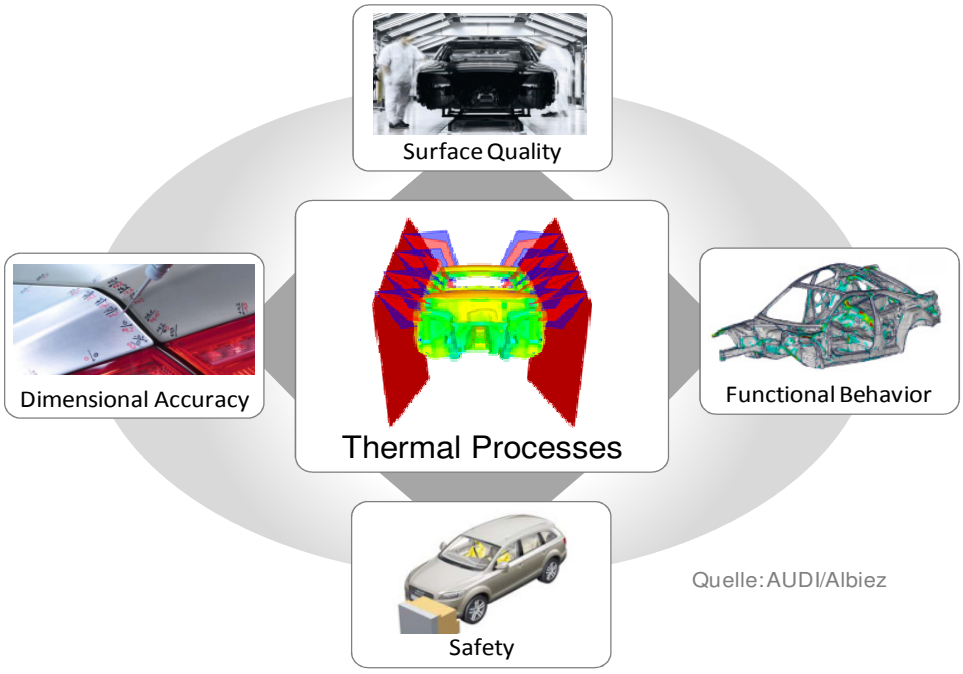

Fig. 2: Influence of thermal processes to the final product characteristics

Furthermore, the heat during coating process is used to increase the yield strength of aluminum alloys (age hardening effect). The increased yield point also has positive effects on the dent resistance and crash performance [1]. However, thermal loads lead to new challenges in the design of joining techniques in car body structures in multi material design. In general, thermal loads in the automotive manufacturing process have a wide range of

influence on the final part characteristics and have to be considered in the early development process of a new product [2].

Challenges

The challenge in the numerical representation of thermal surface distortions is based on the early prediction of the surface quality. A robust prediction of thermal shape distortions is only possible through the exact knowledge of material properties and part characteristics of subsequent process steps. The deep drawing process, lead to sheet thickness distributions as well as shape deviations caused by springback. Additional shape deviations and stress distributions are induced by the assembling process [3]. For this reason, a continuous process simulation including the forming, assembling, transportation and coating process is necessary [4, 5].

The numerical prediction of shape deviations due to thermal loads is based on thermal stress FE-Analysis. Figure 3 illustrates a sequentially coupled thermal stress simulation procedure

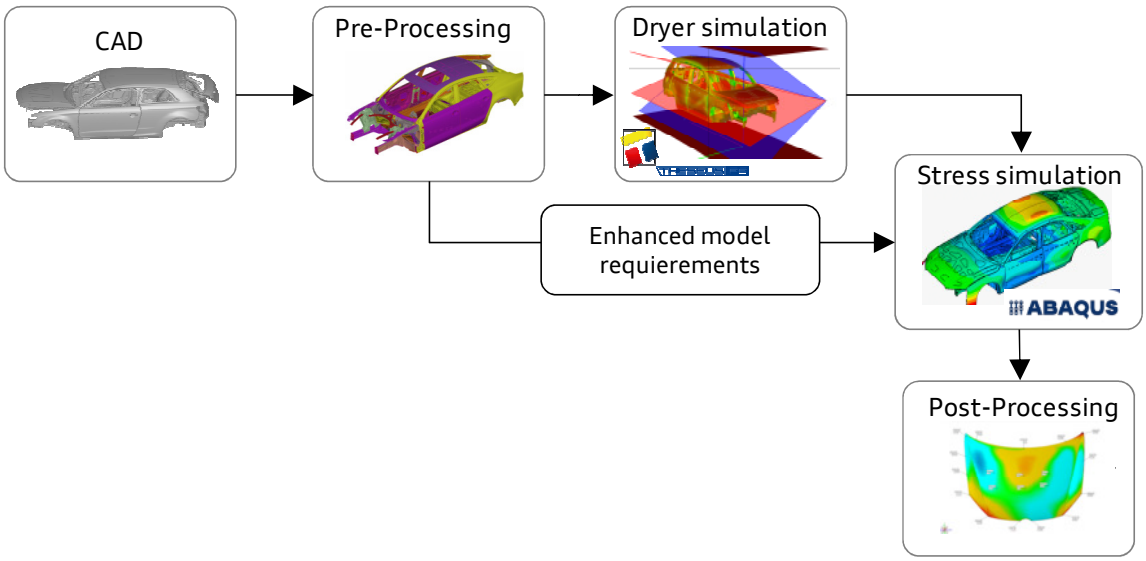

Fig. 3: Sequentially coupled thermal stress simulation procedure

The simulation procedure starts with the pre-processing of the FE-model. Whereby the FE mesh is generated based on nominal CAD data. In consecutive steps, material and part properties have to be defined and assigned to the specific parts. To simulate the heating process, hang on parts have to be modified in the opening angles and distance devices are implemented in order to represent the real coating set up. In the next step, the heterogeneous temperature field during the heating process is calculated. The resulting transient temperature field is imported into the stress simulation in the form of thermal loads. In the stress simulation, the FE-model has to be modified in terms of contact conditions and joining techniques. In the post-processing step, the results are visualized and evaluated.

To calculate the thermal car body deformation behavior, temperature dependent material properties have to be considered. Here, special attention has to be paid to define the yield point. Passing the yield point leads to local plasticization and irreversible deformation in outer shell panels. For this reason, the focus on this work is put on the determination of the yield point and subsequent flow behavior.

Coating process

During the coating process the car body passes through several heating steps. After the pretreatment and cathodic electrodeposition (CED) the car body is heated up to ~200°C for 20 minutes to cure CED coating (Figure 4).

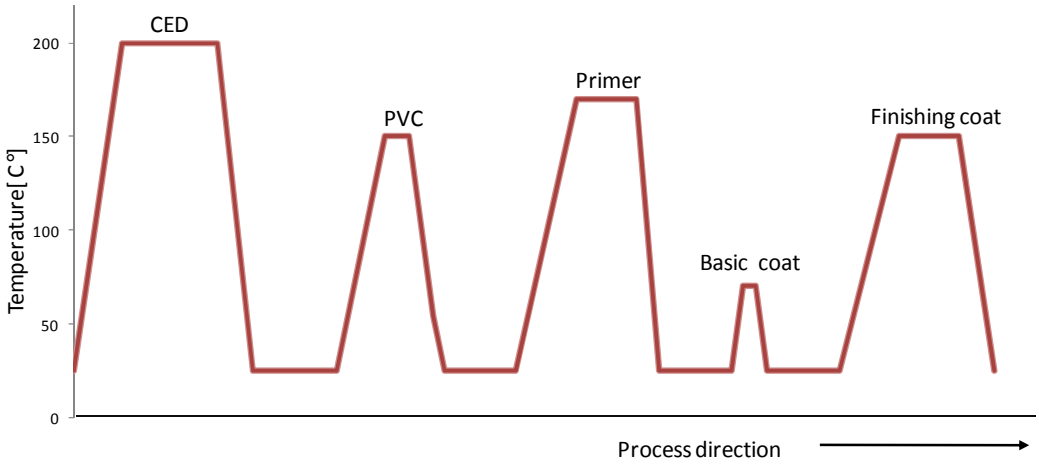

Fig. 4: Simplified temperature profile

As illustrated in the temperature profile (Figure 4) the car body passes through the PVC, Primer, Basic coat and Finishing coat dryer after the CED coating process. The PVC dryer is used to cure the PVC seam sealing for 10 minutes at ~150°C. After the sealing the primer coat is applied on the car body. The aim of the primer layer is to compensate surface unevenness. The curing takes 15 minutes at ~170°C. In the next step, the basic coat is applied. The basic coat is the color-providing layer and available in different uni and metallic colors. The basic coat is just shortly heated up for 3 minutes at ~65°C to provide a better adhesion for the finishing coat. The finishing coat serves for protection of environmental influences and is cured for 15 minutes at ~150°C.
All dryer in the coating process are built as convective dryers, hereby the car bodies are heated up by hot air nozzles and cooled down by corresponding cold air nozzles [6].

Numerical representation of drying processes

The numerical representation of transient temperature fields within the coating process may be calculated by computational fluid dynamics simulations (CFD) as well as by empirical equivalent models. Due to lower simulation costs, the equivalent models such as VPS/Dry or Theseus FE Oven have been established in the automotive industry [7, 8]. The equivalent temperature model describes the entire heater layout including the position and angle of the hot air nozzles, and radiation walls (see Figure 5).

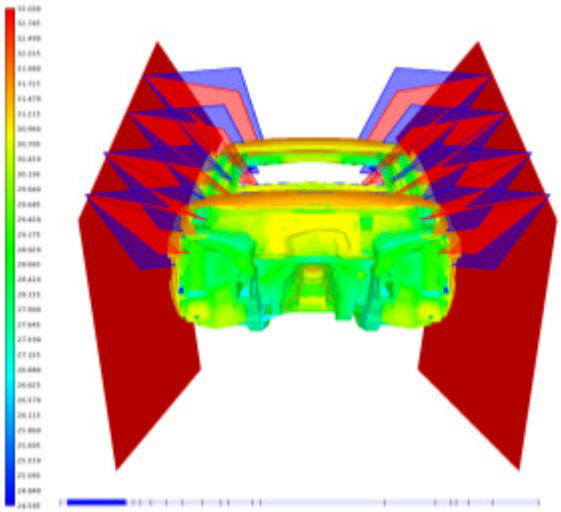

Fig. 5: Temperature field calculation using equivalent temperature model [Audi]

The equivalent model uses a ray tracing technology to calculate the object temperature for every single element in the FEM model. The ray tracing algorithm tests whether the element is in the influencing area of a hot air nozzle, affected by recirculation air or inside the car body structure. In relation to the environment, every finite element receives a specific element temperature due to forced convection or ambient temperature. Within the heat transfer calculations, thermal conduction effects and radiation are considered as well.

The temperature field obtained after the thermal calculation is illustrated in Figure 6.

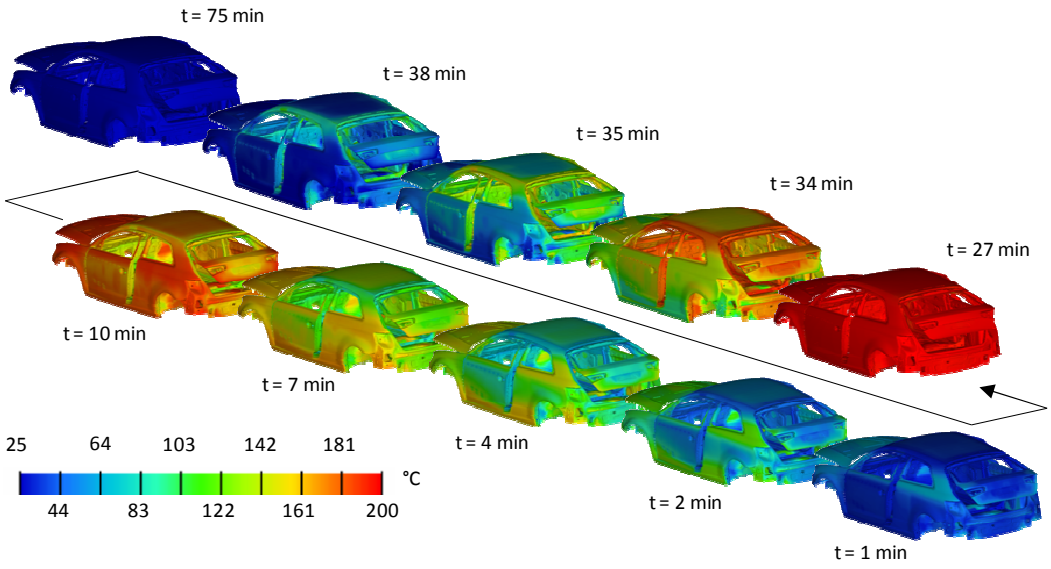

Fig. 6: Calculated temperature field [Audi]

In the following structural FEM simulation (Figure 3) the transient temperature fields are used to calculate the thermal deformation. The surface deflection originates due to linear expansion under the application of heat. If the thermal expansion is suppressed, the internal stress may lead to stability problems [9]. Combinations of materials with different expansion coefficients, such as aluminum and steel alloys, increase this effect even more [10].

Investigated material and testing procedure

In the automotive industry 6xxx series aluminum alloys are formally used for outer shell panels. Such age-hardenable AlMgSi alloys provide a good formability combined with high strength and excellent corrosion resistance. The target yield strength is obtained by heat treatment during paint baking [11]. The material is transformed from the initial state T4 after shipment into the T6 state [12]. In a so-called "lean-process" the age-hardening is greatly accelerated by reheating the material to temperatures of about 95°C-205°C. [13]

To investigate the thermal deformation behavior of car body structure, the knowledge of material behavior is of particular importance. For this reason, the thermo mechanical material properties at different temperature levels and various hardening steps in the CED-heating process were investigated. In further studies the effect of initial age-hardened state after shipment (so-called state T4) by varying heat treatment duration and pre-stretching to the final yield strength (so-called state T6) was investigated.

The specific area of interest is displayed in figure 6. Area 1 deals with temperature depended flow curve on different temperature levels and the implementation into FE-Analysis. In Area 2 the effect of time dependent precipitate hardening at specified temperature of 200°C was investigated. The effect of pre-age hardened and pre-stretched specimen as well as following temperature steps (Figure 4) to the final yield strength (T6) at room temperature (~25°C) is examined in area 3.

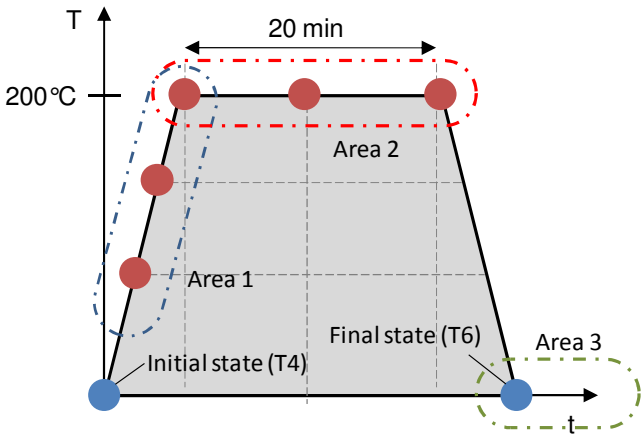

Fig. 7: Area of interest for material properties

The determination of temperature dependent flow curves are performed by using uniaxial tensile tests according to DIN EN ISO 6892-1 and DIN EN 10002-5 for tensile tests at higher temperatures. All tensile tests are executed by using a Zwick tensile testing machine with a maximum speed of $0.1s^{-1}$. The obtained stress strain curves at different temperatures are illustrated in Fig. 8.

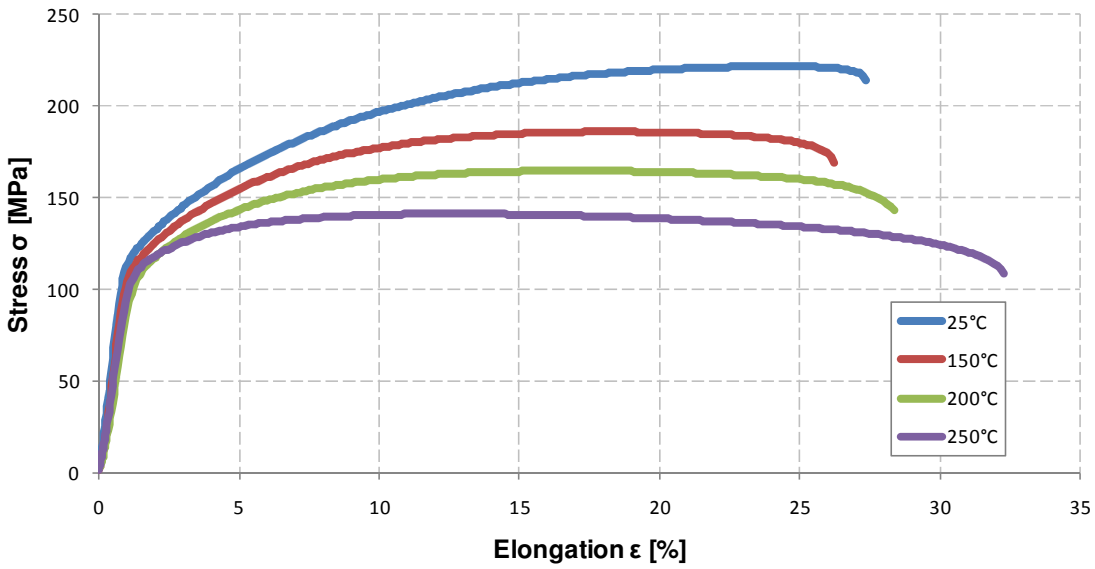

Fig. 8: Stress strain curves of AA6016 at different temperatures

For the implementation of the determined experimental data into a FEA (finite element analysis), the curves have to be converted from engineering stress and strain into true stress and strain.
To avoid numerical problems because of large strain effects in elements next to boundary conditions the experimental data has to be extrapolated to higher strain values. For the extrapolation procedure, several extrapolation rules are available.

In the technical literature following flow curve extrapolation rules are mentioned. In all cases, the equations are designed for prediction of flow curves at ~ 300 K. The well-known equation for flow curve description is defined by Ludwik and Hollomon [14, 15].

$$\sigma(\varphi) = K\varphi^n \tag{1}$$

In this connection the flow curve extrapolation is described by true strain ϕ with n-value (hardening coefficient) in the exponent, multiplied by a coefficient K.
Swift published another equation (2), here $\bar{\varepsilon}^0$ (initial strain value) is taken into account in the description [16].

$$Y(\bar{\varepsilon}^p) = \mathrm{K}(\bar{\varepsilon}^0 + \bar{\varepsilon}^p)^n \tag{2}$$

In this formulation, the flow curve extrapolation is shifted to higher initial values φ_0.

This approach has been modified by Backofen and Ghosh in 1973 [17]. Here, the original equation is completed by adding a constant factor C in equation 3

$$Y(\bar{\varepsilon}^p) = \mathrm{K}(\bar{\varepsilon}^0 + \bar{\varepsilon}^p)^n - \mathrm{C} \tag{3}$$

Voce published in 1948 a further flow curve extrapolation description [18]. In this equation (4), Voce includes the plastic strain variable ε_{pl} in the exponent.

$$\sigma(\varepsilon_{pl}) = A - B \cdot \exp(-C \cdot \varepsilon_{pl}) \tag{4}$$

The constant parameters A, B and C have to be determined experimentally.
Armstrong, Hocket and Sherby have modified the approach of Voce by implementing an additional parameter d in the exponent of plastic strain value $\varepsilon_{\mathrm{pl}}$ [19]

$$\sigma(\varepsilon_{pl})_f = a - b \cdot \exp\left(-c \cdot {\varepsilon_{pl}}^{d}\right) \tag{5}$$

The results of the extrapolated flow curves are represented for the experimental data at temperature of ϑ =200°C in figure 8. Hereby, the tensile tests are performed immediately after reaching the desired temperature contrary to DIN EN 10002-5 to avoid precipitate hardening during the heat treatment.

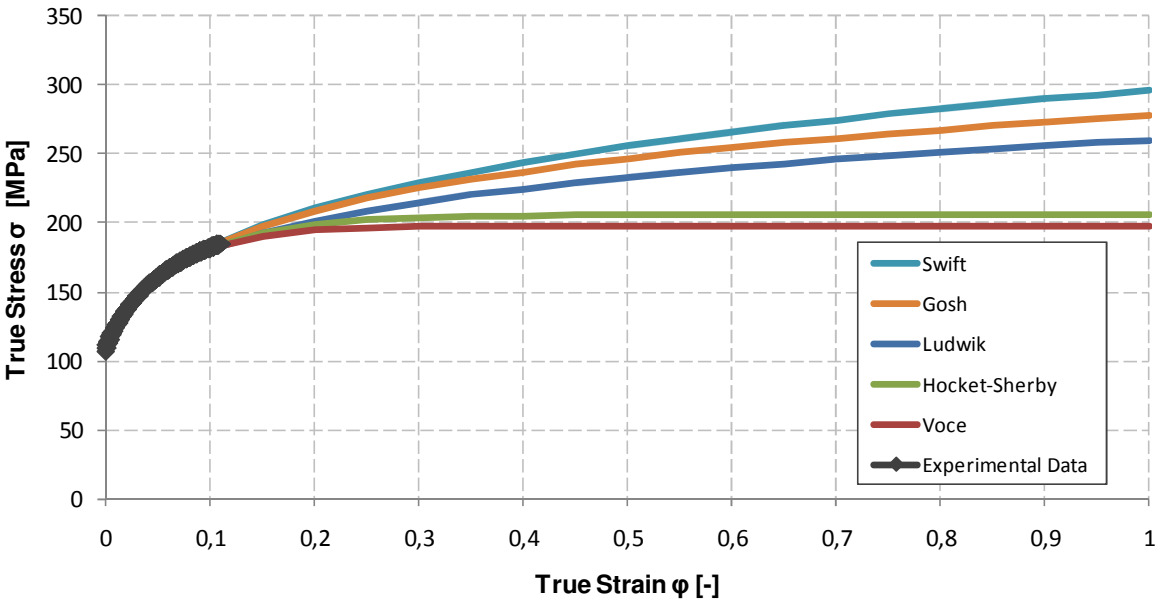

Fig. 9: Flow curve extrapolation at ϑ =200°C using different extrapolation approaches for AA6061 aluminum alloy

As illustrated in Fig. 9, there is a significant difference in the achieved flow curves using the described extrapolation rules. According to the results, the selection of extrapolation rules at higher strain values $\varphi > 0{,}2$ have to be considered. The most critical flow curve characteristic in a FEA can be modeled by the extrapolation rule of Voce.

Precipitation hardening of AA6016 alloys

In the following, the material behavior according to Figure 7 (Area 2) is investigated. Here, the hardening behavior at maximum temperature during the heat treatment is of particular interest.
In age-hardenable alloys, strengthening is caused by the precipitation of second phases, and their interaction with dislocations. Precipitates obstruct the movement of dislocations through the matrix and hence increase the stress necessary for plastic deformation of a material [20]. Under the influence of an externally imposed stress, dislocations can shear small precipitates to permit plastic deformation. The additional required shear stress for the cutting of a precipitate is proportional to the square root of its radius r. The larger the precipitate, the greater the obstruction to dislocation motion it presents. If the precipitates

grow to exceed a critical size, bowing around a precipitate is energetically favorable to cutting it. According to the theory first described by Orowan, the required shear stress for a dislocation to loop around a precipitate is inversely proportional to the edge-to-edge distance between precipitates [21].
A mathematical model to predict the age hardening behavior of AlMgSi alloys was developed by Myhr et al. [22]. Gouttebroze et al. and Briol developed more sophisticated models in their scientific work, where the development of microstructure is characterized by a complex sequence of hardening processes [23, 24]:

Supersaturated solid solution → Mg and Si Cluster → GP Zones → β''→ β'→β

At present, the evolution of precipitation of meta stabile phases can be calculated by means of simulation Software MatCalc, which has been developed by Kozeschnik et al [25].
In this work, the hardening behavior of AA6016 is investigated by experimental data using the uniaxial tensile test. The AA6016 alloy exhibits an initial yield strength of $\sigma_{y,i} = 124\ MPa$ with a sheet thickness of 1.04mm. Contrary to the existing standard of DIN EN 10002-5, the specimens are heated up to the desired temperature of 200°C. As soon as the specimen reaches their temperature level, the uniaxial tensile test is performed. The results achieved in the form of stress strain curves are displayed in Figure 10 for one selected curve (200°C_0min).

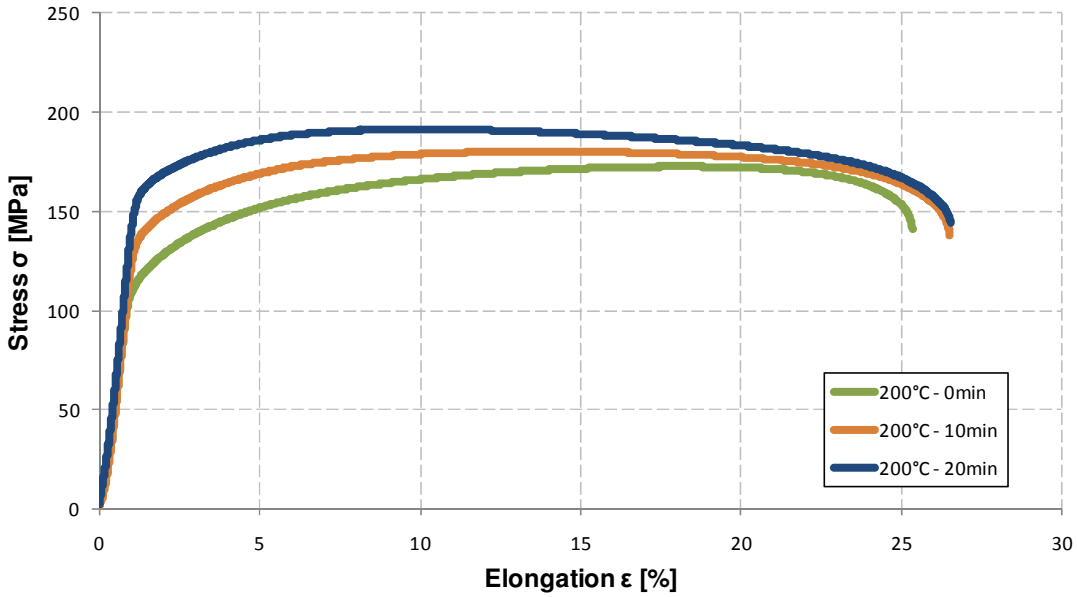

Fig. 10: stress strain curves of AA6016 at 200°C with different precipitation states

In the following steps, the tensile tests are performed at 200°C after 10 minutes and 20 minutes. Compared to the initial yield strength of $\sigma_{y,i}(25℃, 0) = 124\ MPa$, the yield strength decreases by reaching 200°C to $\sigma_y(200, 0) = 111\ MPa$. While holding the temperature up to 200°C the yield strength increased to $\sigma_y(200, 10) = 140\ MPa$ after 10 minutes. After 20 minutes, the precipitate hardening of the Mg_2Si phase lead to a yield strength of $\sigma_y(200, 20) = 161\ MPa$. Comparing the mechanical properties of AA6016 in Figure 11, the tensile strength σ_{TS} increases, whereas the uniform elongation ε_u decreases.

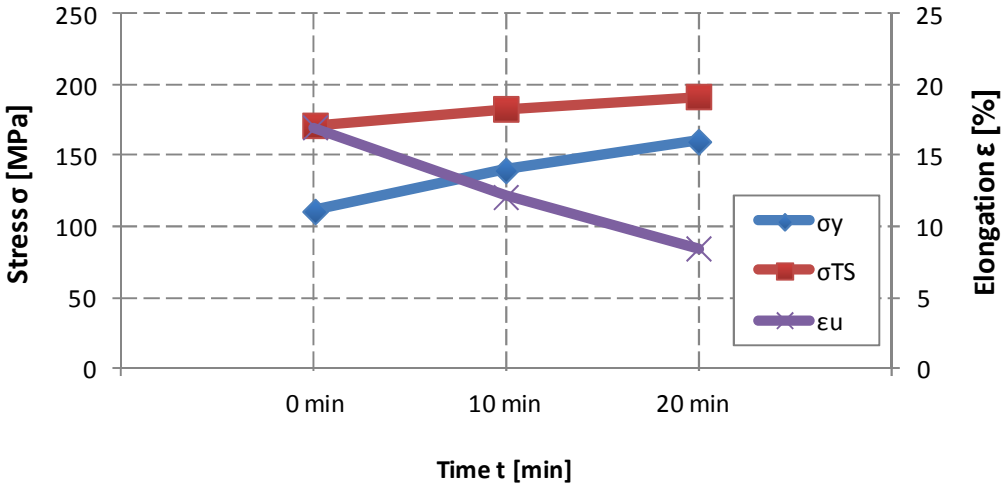

Fig. 11: Mechanical properties of AA6016 at 200°C as function of hardening time

Furthermore, Figure 11 points out, that the slope of increasing tensile strength $\sigma_{TS}\ (\vartheta, t)$ is less than the yield strength $\sigma_y(\vartheta, t)$. The results achieved are $\sigma_{TS}(200, 0) = 172\ MPa$, $\sigma_{TS}(200, 10) = 183\ MPa$ and $\sigma_{TS}(200, 20) = 183\ MPa$. However, the result points to a significant effect in terms of the uniform elongation $\varepsilon_u(\vartheta, t)$. The uniform elongation starts with $\varepsilon_u(200, 0) = 17\%$ by reaching 200°C temperature level and drops to $\varepsilon_u(200, 10) = 12\%$ after 10 minutes until $\varepsilon_u(200, 20) = 8\%$ after 20 minutes.

Implementing this behavior into a FE-Analysis the yield point and the flow curves have to be defined as function of heat and time. The behavior of a time dependent isotropic yield surface (von Mises) at 200°C with regard to the experimental data is illustrated in Figure 12.

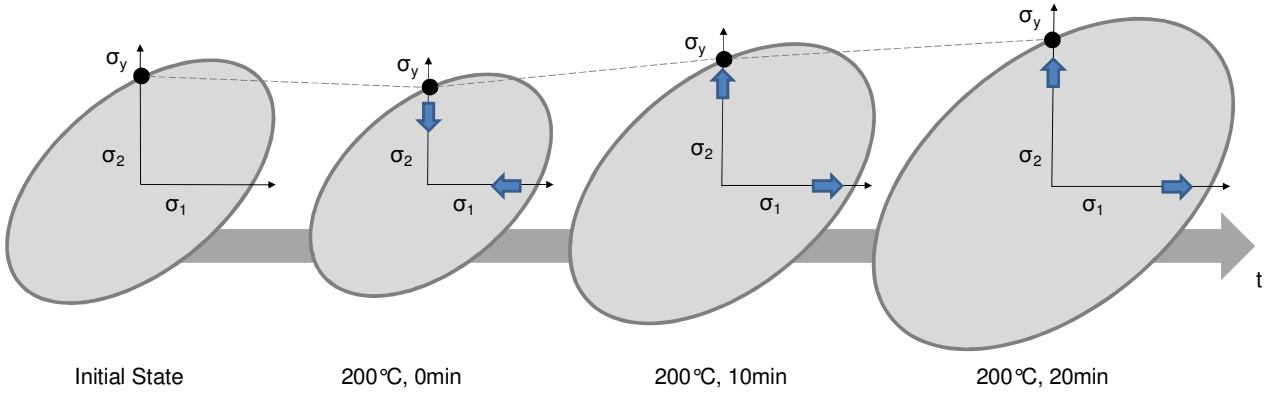

Fig. 12: Heat and time dependent evolution of yield surface

Beside the yield surface, the specific flow characteristics according to Figure 10 have to be implemented into the FE-Analysis. In the investigation of car body structures in thermal processes, the most critical state can be defined by reaching the maximum temperature level (200°C, 0min).

In further investigations according to area 3 in Fig. 7 the influence of initial yield strength, pre-stretching and subsequent thermal loads to the final yield strength is dealt with.

Influence of initial yield strength

The difference in the initial yield strength values is attributed to the natural ageing behavior of AA6016 alloys during storage. As material for this investigation served two AA6016 alloys, alloy A and alloy B, with a sheet thickness of 1.04 mm. Alloy A has an initial yield strength of $\sigma_{yA,i} = 114\ MPa$, whereas alloy B has an initial yield strength of $\sigma_{y,Bi} = 125\ MPa$. Both alloys are hardened at 200°C up to 20 minutes. The results achieved after heat treatment are illustrated in Figure 13.

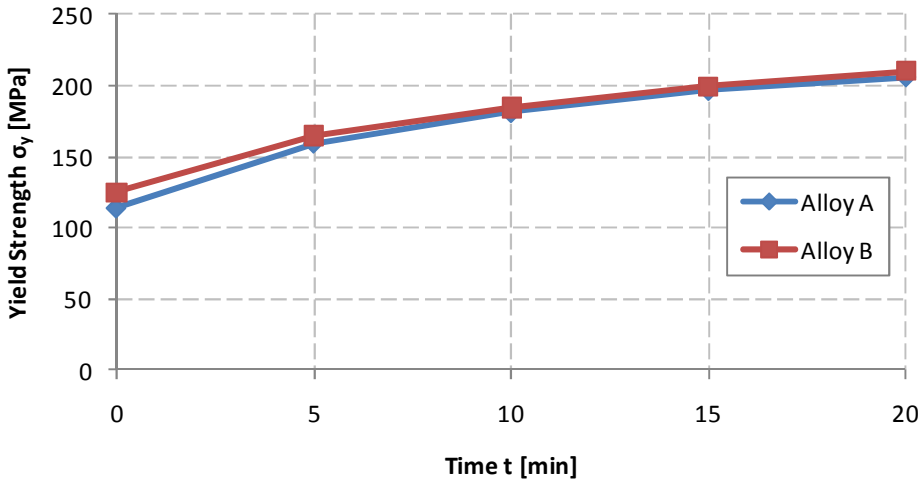

Fig. 13: Hardening evolution of AA6016 alloys with different initial yield strength.

Alloy A and B exhibits similar hardening tendencies. Here, the former difference of $\Delta\sigma_{y,i} = 11\ MPa$ has decreased to $\Delta\sigma_{y,20} = 4\ MPa$ after a heat treatment of 200°C for 20 minutes. Thus the initial difference is compensated by the hardening process.

Influence of pre-stretching

Considering upstream processes, such as sheet metal forming, the effect of pre-stretching to the final yield strength was investigated. Hereby, an AA6016 alloy with an initial yield strength of $\sigma_{y,i} = 114\ MPa$ and sheet metal thickness of 1.04 mm was used. The pre-stretching levels were defined in three steps: 0%, 2%, 5%. All specimens were heated up to 200°C. Figure 14 represents the results at different heat treatment durations.

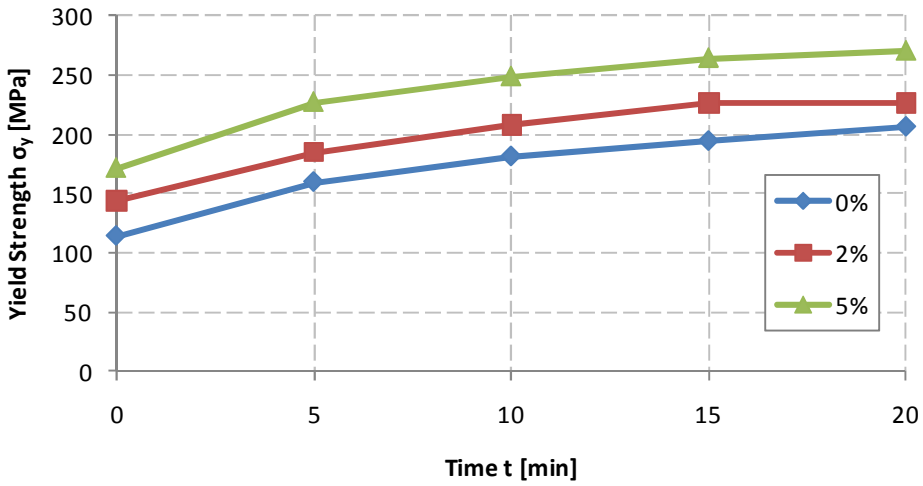

Fig. 14: Yield strength of AA6016 (Alloy A) as function of different pre-stretching levels

The representation points the positive effect of pre-stretching to the final yield strength σ_y. In this investigation the displayed curves with pre-stretching levels of 0%, 2%, 5% exhibit an equivalent hardening tendency. The specimen without pre-stretching increases from $\sigma_{y,i,0} = 114\ MPa$ to $\sigma_{y,0} = 206\ MPa$. After pre-stretching of 2% the specimen achieved an initial yield strength of $\sigma_{y,i,2\%} = 144\ MPa$ and concludes at a final yield strength of $\sigma_{y,2\%} = 226\ MPa$. The specimen with a pre-stretching level of 5% achieved a final yield strength of $\sigma_{y,5\%} = 270\ MPa$ by an initial yield strength of $\sigma_{y,i,5\%} = 144\ MPa$. Because of determined results, upstream processes as forming operation have to be taken into account to evaluate the final yield strength.

Influence of subsequent thermal processes

According to Figure 4 the influence of subsequent thermal processes to the final yield strength σ_y. is investigated. Therefore, specimen of AA 6016 alloy with an initial yield strength of $\sigma_{y,i,0} = 114\ MPa$ and sheet thickness of 1.04 mm are heat treated along the entire coating process. The results are compared to previous described investigations of the CED temperature profile. Figure 15 illustrates the obtained yield strength σ_y along different pre-stretching levels of 0%, 2%, 5% and 10%. Here, RT indicates the obtained yield strength at room temperature, CED after the first and highest thermal process (CED dryer) and TP (Temperature Profile) after the entire coating process.

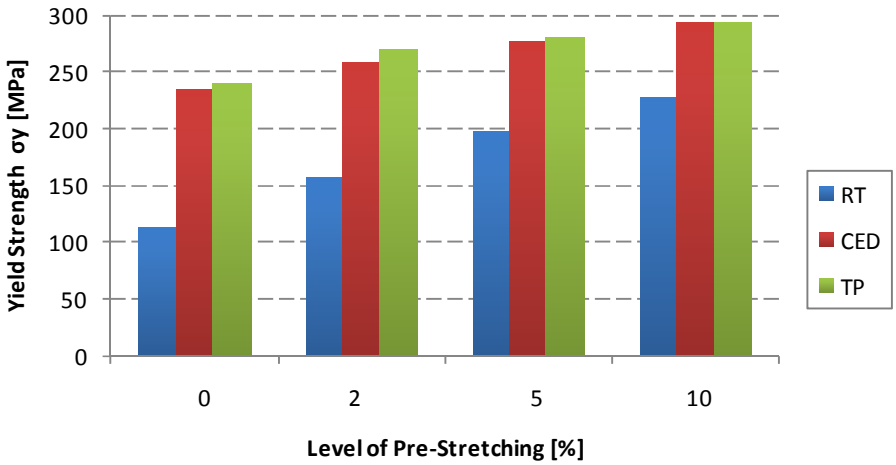

Fig. 15: Obtained yield strength σ_y after different heat treatments

As in Figure 15 displayed, there is no significant increase of the final yield strength σ_y achieved. In fact, the obtained increase considering the entire thermal coating process is less than 5% ($\Delta\sigma_{y,0\%} = 5\ MPa, \Delta\sigma_{y,2\%} = 12\ MPa, \Delta\sigma_{y,5\%} = 4\ MPa, \Delta\sigma_{y,10\%} = 1\ MPa$).
For this reason, the prediction of the final yield strength can be restricted to the CED temperature profile.

Summary and conclusion

In the present paper, the influences of thermo mechanical material characteristics of AA6016 aluminum alloy affecting the thermal deformation behavior during the coating processes were investigated. Here, the prediction of the yield point and the flow curve characteristics is of particular importance for numerical calculations. For this reason, thermo mechanical material properties have been investigated at different temperature levels and heat treatments in terms of varying dwell-times.
The determination of temperature dependent flow curves were performed by using the uniaxial tensile test. In this work, flow curves were determined from room temperature until a temperature of 250°C. The implementation of flow curves into a FEA system requires extrapolated data. Hence, differences of flow curve extrapolation rules were carried out. According to the results, the selection of extrapolation rules at higher strain values have to be considered.
In further studies, the hardening behavior of AA6016 at 200°C was investigated. Tensile test after several dwell-times were performed. The comparison pointed out, that the yield strength σ_y and the tensile strength σ_{TS} increases, whereas the uniform elongation ε_u decreases. This requires a heat and time dependent formulation in the FE-Analysis for the yield point, whereas the most critical situation represents the state before hardening starts at the maximum temperature.
The influence of pre-aging due to storage and batch fluctuations to final yield strength was studied on two alloys. The results demonstrated that initial ageing was compensated by the thermal hardening process.
However, pre-stretching has a significant effect on the final yield strength. Pre-stretching prior to heat treatments (CED dryer) gives an additional benefit with respect to an increased strength. Because of the determined results, upstream processes as forming operations have to be taken into account to evaluate the final yield strength. Whereas the final yield strength

has increased only slightly by taking subsequent thermal processes into consideration. Thus, the prediction of the final yield strength can be restricted to the CED temperature profile. In consideration of the shown connections in this paper, further experimental examination to implement the material behavior into FEA will be accomplished at the Institute for Metal Forming Technology (IFU) in cooperation with the Audi AG.

References

[1] Zöller, A.; Frank, T.; Haufe, A.: Berücksichtigung von Blechumformergebnissen in der Crashberechnung, 3. LS-Dyna Anwenderforum, Bamberg 2004

[2] Albiez, C.; Polzer, A.; Görres, A.; Sindel, M.; Liewald, M.: Bewertung der Oberflächenqualität von Blechbauteilen nach thermischen Prozessen, wt Werkstattstechnik online, Jahrgang 100, Heft 10, S. 743-752, 2010

[3] Neugebauer, R.; Rössinger, M.; Wahl, M.; Schulz, A.; Eckert, A.; Schützle, W.: Predicting dimensional accuracy of mechanically joined car body assemblies, Internationale Konferenz für Belchumformung, SheMet 2011, Leuven, Belgien, 2011

[4] Awiszus, B.; Bolick, S.; Pinner S.: Durchgängige Simulationsprozessketten in der Fahrzeugentwicklung, International Konferenz „Neuere Entwicklungen in der Blechumformung“, Fellbach,2010

[5] Albiez, C.; Liewald, M.; Görres, A.; Regensburger, J.: Enhanced requirements for surface quality of outer car body shells according to thermal manufacturing processes,Internationale Konferenz für Belchumformung, SheMet 2011, Leuven, Belgien, 2011

[6] Braess, H.; Seiffert U.: Vieweg Handbuch Kraftfahrzeugtechnik, 4. Auflage, ATZ/MTZ-Fachbuch, Vieweg Verlag, Wiesbaden, ISBN 3-528-33114-3, 2005

[7] Blanke, D.: Modellierung und numerische Simulation des Aufheizverhaltens von PKW-Bauteilen und –Karosserien, Dissertation, Technische Universität Darmstadt, 2009

[8] Yu-Ning, L.: Advanced Manufacturing Technology Development, Ford Motor Company Dearborn, Michigan, USA, 22nd CAD-FEM Users' Meeting 2004, International Congress on FEM Technology with ANSYS CFX, International Congress Center Dresden, 2004

[9] Paulke, S.: Ein Betrag zur Herleitung und Lösung nichtlinearer, thermomechanisch gekoppelter Grundgleichungen für Schalentragwerke, PhD Thesis, Universität der Bundes-wehr München, 2002

[10] Irretier, A.: Sonderforschungsbereich 570 „Distortion Engineering“, Projekt C1 – Stoffwertebestimmung, Schlussbericht, 2009

[11] Furrer, P.; Bloeck, M.: Kosteneffizienter Leichtbau – realisiert mit Aluminium, 5. Chemnitzer Karosseriekolloquium CBC, 2008

[12] F. Ostermann, Anwendungstechnologie Aluminium, 2. Auflage, Springer Berlin Heidelberg New York, Germany, (2007)

[13] Hatch, J.: Aluminum: properties and physical metallurgy, American society for metals, metals park, 1984

[14] Ludwik, P.: Elemente der technologischen Mechanik, Springer Verlag, Berlin, 1909

[15] Hollomon, J. H.: Tensile deformation. Trans. Met. Soc. AIME 162, pp 2668-290, 1945

[16] Swift, H.W.: Plastic instability under plane stress, Journal Mech. Phys. Solids, Vol. 1, pp. 1-8, 1952

[17] Backofen, W.A.; Gosh, A.K.: Strain Hardening and Instability in Biaxially Stretched Sheets. Metallurgical Transactions, Vol. 4, pp. 1113-1123, 1973

[18] Voce, E.: J. Inst. Met., Vol. 74, pp. 537-562, 1948

[19] Armstrong, P.E.; Hocket J.E.; Sherby O.D.: Large strain multidirectional deformation of 100 aluminium at 300K, Journal of the Mechanics and Physics of Solids, Vol. 30

[20] Callister, W.D: Materials science and engineering, Wiley, New York, 2003

[21] Gottstein, G.: Physical Metallurgy, Virtual production of industrial aluminium production. Wiley-VCH, 2006

[22] Myhr, O.R.; Grog, O.: Modelling of the age hardening behavior of Al-Mg-Si alloys, Acta Materialia Vol. 49, pp.65-75, 2001

[23] Gouttebroze, S.; Mo, A.; Grog, O.; Peterson, K.O; Fjaer, H.G.: A new Constitutive Model for the Finite Element Simulaiton of Local Hot Forming of Aluminum 6xxx Alloys, Metallurgical and Materials Transactions A, Vol. 49, pp. 522-534, 2008

[24] Briol, Y.: DSC analysis of the precipitation reactions in the alloy AA6082: Effect of sample preperation, Journal of Thermal Analysis and Calorimetry, Vol. 83, pp. 219-222, 2006

[25] Kozeschnik, E.; Svoboda, J.; Fischer, F.D.; Fratzl, P.: Modelling of kinetics in multi-component multi-phase systems with spherical precitipates. Materials Science and Engineering A, Vol. 385, pp. 166-174, 2004

Dipl.-Ing. Christoph Albiez, Prof. Dr.-Ing. Mathias Liewald MBA
Institut für Umformtechnik (IFU)
Universität Stuttgart
Holzgartenstraße 17, D-70174 Stuttgart
Tel. +49 (0)711 685-782302
Fax. +49 (0) 711 685-83839
E-mail: christoph.albiez@ifu.uni-stuttgart.de
www.uni-stuttgart.de/ifu

Dipl.-Wirtsch.-Ing. Andreas Görres (FH), Dipl.-Ing. Jochen Regensburger
Audi AG
NSU-Straße, D-74148 Neckarsulm
Tel. +49 (0)7132 31-72472
Fax. +49 (0)7132 31-84-72472
E-Mail: andreas.goerres@audi.de
www.audi.de